Optical Engineering

OpticalEngineering.SPIEDigitalLibrary.org

# Femtosecond laser-written double-cladding waveguides in $Nd:GdVO_4$ crystal: Raman analysis, guidance, and lasing

Hongliang Liu
Javier R. Vázquez de Aldana
Magdalena Aguiló
Francesc Díaz
Feng Chen
Airán Ródenas Seguí

SPIE.

# Femtosecond laser-written double-cladding waveguides in Nd:$GdVO_4$ crystal: Raman analysis, guidance, and lasing

**Hongliang Liu,[a] Javier R. Vázquez de Aldana,[b] Magdalena Aguiló,[c] Francesc Díaz,[c] Feng Chen,[a,*] and Airán Ródenas Seguí[c]**

[a]Shandong University, School of Physics, State Key Laboratory of Crystal Materials and Key Laboratory of Particle Physics and Particle Irradiation (Ministry of Education), Jinan 250100, China
[b]Universidad de Salamanca, Laser Microprocessing Group, Departamento Física Aplicada, Facultad Ciencias Físicas, Salamanca 37008, Spain
[c]Universitat Rovira i Virgili, Departament de Química Física i Inorgànica, Tarragona 43007, Spain

**Abstract.** We report on waveguide lasers at 1064.5 nm in femtosecond laser-written double-cladding waveguides in Nd:$GdVO_4$ crystals. The cladding waveguides guide both transverse electric (TE)- and transverse magnetic (TM)-polarized modes with considerably symmetric single-modal profiles and show good transmission properties (propagation loss as low as 1.0 dB/cm). The detailed structure of the single and double claddings has been imaged by means of $\mu$-Raman analysis, and the observed slight fabrication asymmetries with respect to an ideal circular cladding are in well agreement with the observed differences in TE/TM propagation losses. Importantly, the Raman imaging shows the complete absence of lattice defect at the laser active volume. Under the optical pumping at 808 nm, a maximum output power up to 0.43 W of the continuous wave waveguide laser with a slope efficiency of 52.3% has been achieved in the double-cladding waveguide, which is 21.6% and 23% higher than that from a single-inner cladding waveguide. Furthermore, the maximum output power of the waveguide laser is 72% higher than that of the double-line waveguide due to the double-cladding design.  [DOI: 10.1117/1.OE.53.9.097105]

Keywords: optical waveguides; laser material processing; waveguide lasers; Raman spectroscopy.

Paper 141083P received Jul. 7, 2014; revised manuscript received Aug. 13, 2014; accepted for publication Aug. 14, 2014; published online Sep. 9, 2014.

## 1 Introduction

Optical waveguide structures are the fundamental elements in integrated photonics and modern telecommunication systems, in which light could be confined in very small volumes.[1] Compared with the bulk material, relatively high-optical intensities could be reached in the structures. Benefiting from the compact geometry and compressed intracavity intensity, waveguide lasers possess a number of advantages, such as reduced lasing thresholds and comparable efficiencies, with respect to bulk laser systems.[2] Three-dimensional (3-D) femtosecond (fs) direct laser writing (DLW) has become a powerful and promising technique to fabricate optical waveguides in various transparent optical materials,[3–5] since the pioneering work of Davis et al. in 1996.[4] More importantly, compared with other techniques, such as ion implantation, proton exchange, or surface etching techniques, the fs-pulse DLW technique offers the unique capability of constructing true 3-D waveguide circuits with spatial resolution down to ~100 nm from the combination of modern sophisticated 3-D translation stages and laser precision. The achievable types of index changes in a transparent material include the case of so-called Type I waveguides (also called directly written structures, typically with single or multiline writing, with positive refractive index change in the written tracks to fabricate flexible graded-index or step-index profiles, but difficult to find the fabrication conditions from one material to another), Type II waveguides (also called stress-induced waveguides, typically with double-line geometry, locating a confined mode in the region between two filaments, with negative refractive index changes that act as horizontal cladding and with a stress-optic index increase in the center that allows for channel confinement), and depressed cladding waveguides (also called Type III configuration, typically locating a core surrounded by a number of low-index fs-laser written filaments).[6] Type I and Type II structures have been realized in crystals such as YCOB[7] and $LiNbO_3$[8] for Type I waveguides and YAG,[9–14] GGG,[15] $LiNbO_3$,[8] and vanadates[16,17] for Type II waveguides. Compared with Type I structures, the depressed cladding waveguides possess a few unique features such as good thermal stabilities and the well-preserved bulk features in the waveguide area. The geometry of the structures could be designed in almost arbitrary shape with flexible scales, which may result in the high coupling between the optical fibers and waveguides.[18] In addition, the guidance of light at longer wavelength (e.g., at mid-infrared) is realizable for larger-diameter cladding waveguides,[19,20] which is not possible for Type II waveguides. More interestingly, the Type III cladding waveguides may support relatively balanced guided modes along both transverse electric (TE) and transverse magnetic (TM) polarizations, which is one of the unique features of depressed cladding waveguides. As of yet, Type III cladding waveguides have already been fabricated in a number of optical materials, e.g., Nd:YAG single crystals and ceramics,[14,20,21] $BiB_3O_6$,[22] Nd:$YVO_4$,[23] Nd:LGS,[24] and ZBLAN glass.[18,25,26]

Neodymium-doped gadolinium vanadate (Nd:$GdVO_4$) is one of the well-known rare-earth ion-doped gain media for solid-state laser systems. It is also known to be an efficient

*Address all correspondence to: Feng Chen, E-mail: drfchen@sdu.edu.cn

0091-3286/2014/$25.00 © 2014 SPIE

$\chi^{(3)}$-material for ultrashort-pulse Raman lasers[27] through stimulated Raman scattering (SRS) processes. Owing to its high-thermal conductivity, high-damage threshold, and excellent spectroscopic properties, specially to the higher laser slope efficiencies compared with the Nd:YAG or Nd:$YVO_4$ gain media, Nd:$GdVO_4$ crystal is of great relevance for the development of solid-state lasers.[28–30] Channel waveguides have been fabricated in Nd:$GdVO_4$ crystals by swift heavy-ion irradiation,[31] pulse laser deposition,[32] and double-line fs-laser inscription.[17] In this work, we report on the fabrication of Nd:$GdVO_4$ circular cladding waveguides constructed with multiple fs-laser damage tracks and the efficient continuous wave (cw) output laser oscillation at 1064.5 nm in the cladding waveguides. We compare the guiding properties and laser performances of the waveguides fabricated with different volume configurations.

## 2 Experiments Details

The a-cut Nd:$GdVO_4$ crystal sample (doped by 2 at.% $Nd^{3+}$ ions) was cut with sizes of $2 \times 3.7 \times 8$ $mm^3$ along $a$, $b$, and $c$ axes, respectively. The circular-depressed double-cladding waveguides were produced by using the laser facility of the Universidad de Salamanca, Spain, in which a system of a Ti:Sapphire regenerative amplifier (Spitfire, Spectra Physics, Santa Clara, California) was used as a laser source. It delivered linearly polarized pulses of 120 fs and 795-nm central wavelengths at a 1-kHz repetition rate as in previous works.[17,21–24] The maximum available pulse energy was 1 mJ, but it was reduced with a calibrated neutral density filter placed after a half-wave plate and a linear polarizer, in order to get a fine control of the incident energy.

During the fabrication process of the tubular cladding waveguides, the pulse energy was set to 1.68 $\mu$J, the laser beam was focused with a 40× microscope objective (NA ~0.65) to an approximate 1.5-$\mu$m diameter focal spot at $1/e^2$, and the focusing depth was set at 150 $\mu$m beneath one of the $8 \times 4$ $mm^2$ surfaces. The sample was scanned at a constant velocity of 500 $\mu$m/s in the direction parallel to the 4-mm edge, producing a damage line along the sample. This scan speed implies a pulse-to-pulse spatial separation of around 500 nm and a spot overlapping of around 66%, which means that the stress accumulation is strongly minimized while maintaining a continuous cladding track. The laser writing process under a 1-kHz repetition rate can also be considered as a cold laser inscription process, because each incoming pulse is separated from the rest by an arrival time of 1 ms, which is much longer than the cooling time of the focal volume (around 0.5 $\mu$s). The absence of any thermal accumulation and annealing implies that the writing process will induce maximum crystal lattice damage (refractive index decrease) at the cladding. The line scan procedure was repeated consecutively at different depths and lateral positions of the sample, following the desired circular geometry, as the design shown in Fig. 1(a), with a lateral separation of 3 $\mu$m between each two adjacent tracks. Under these conditions, a depressed-double-cladding waveguide with cross-sectional diameters of 150 $\mu$m for out cladding and 30 $\mu$m for inner cladding structures (hereby referring to waveguide WG1), and for comparison a single inner cladding configuration with diameter of 30 $\mu$m, was also fabricated [see Figs. 1(b) and 1(c) for images of the cross-sections], respectively. Some cracks can be observed

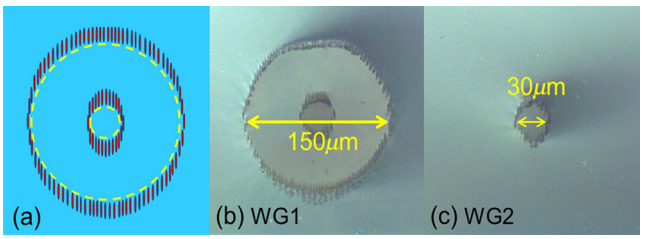


**Fig. 1** Double-cladding waveguides in Nd:$GdVO_4$ at cross-section: (a) schematic plot, microscopic images of the double-cladding waveguide (b) with diameters of 150 and 30 $\mu$m and single-cladding waveguide (c) with a diameter of 30 $\mu$m.

under the microscope at the surroundings of the waveguides because of the large stress induced in the crystal, but they do not affect the waveguide core.

With the measurement of the NA of the waveguides and using the formula reported before,[8] we obtained the maximum change of refractive index of the waveguides, which was estimated to be $2 \times 10^{-3}$. In spite of the method itself being a rough estimation, this value was in good agreement with those reported for other cladding waveguides.[13,17–23] The backreflection method[33] was used to measure the propagation losses of the cladding waveguides at a visible wavelength of 632.8 nm with a polarized He-Ne laser as a light source. For the depressed double-cladding waveguides (WG1), the propagation losses for TE-mode propagation were determined to be ~0.9 dB/cm. Meanwhile, the TE mode loss of WG2 (inner cladding alone) at 632.8 nm was slightly higher of ~1.1 dB/cm. The difference in propagation losses between TE- and TM-polarized modes is within 15% for all cases, that is to say, the transmission loss at TE polarization was lower than that at TM polarization.

Polarized confocal $\mu$-Raman surface mapping characterization of the waveguide facets was also performed using a Renishaw inVia Reflex microscope attached to a 514-nm Argon laser and a 50× focusing Leica objective. Spectral data analysis was performed with WiRE 3.4 Renishaw software. The $A_{1g}(\nu_1)$ phonon mode was analyzed following previous $\mu$-Raman investigations in DLW-fabricated waveguides in Nd:$GdVO_4$.[17] A tunable cw Ti:Sapphire laser (Coherent MBR PE, Santa Clara, California), which generated a polarized light pump beam at 808 nm, was used in the end pumping system to perform the cw waveguide laser-operation experiments at room temperature. A spherical convex lens with a focal length of 50 mm was used to couple the pump laser beam (with waist radius of ~40 $\mu$m) into the waveguide. To achieve the Fabry-Perot cavity for the 1.06-$\mu$m laser emission in the waveguides, a thin optical film with high reflectivity at 1.06 $\mu$m (>99%) and high transmission at 808 nm (~98%) was coated only on the input end-face of the crystal, while no film or additional mirror was attached on the output face (i.e., the reflectivity of the output end face was 10% due to Fresnel reflection, because the refractive index of the Nd:$GdVO_4$ crystal is ≈2). In this way, the out coupler of the cavity was ~90%. We used a 20× microscope objective lens (NA = 0.4) to collect the generated waveguide lasers and an IR CCD camera to image the laser beam through an aperture. A spectrometer with a resolution of 0.2 nm was used to analyze the emission spectra of the generated laser beam.

## 3 Results and Discussion

### 3.1 *Depressed Cladding Structures and Lattice Distortions Analyzed by $\mu$-Raman Mapping*

Only the energy shifts and broadening of the most SRS-active $A_{1g}(\nu_1)$ phonon mode are presented here. This phonon has been previously assigned to totally symmetric stretching optical vibration modes of the tetragonal $VO_4^{3-}$ ionic groups of the vanadate tetragonal crystal,[34] and therefore its energy blue/red shift can be associated to hydrostatic compression/dilatation of the crystal lattice. In the case of laser-written tracks, it is known, however, that the strain/stress fields surrounding the damage tracks are not isotropic.[35] Normally, a uniaxial compression along the horizontal transverse cross-section of each single track is observed, which comes from the volume expansion of the elongated elliptical shape of the focal volume of the fs pulses. This uniaxial compression along the horizontal transverse axis comes along a dilatation or tensile stress for the perpendicular (vertical) transverse direction. Because this biaxial stress distribution is not equal to hydrostatic pressure, we cannot associate the phonon-mode energy shifts with axial stress as there is no detailed information of how the frequency of the $A_{1g}(\nu_1)$ phonon-mode changes with anisotropic stress fields. Even though, the direct measurement of the Raman shifts along the waveguide cross-sections is extremely important in order to know the spatial extension of lattice distortion, lattice defects, and possible stress-optic attributed index changes. With these means, we have analyzed the two-dimensional cross-sections of three types of cladding waveguides, an outer cladding alone, double-cladding waveguide WG1, and the WG2 inner cladding alone.

Figures 2(a)–2(c) shows the cladding structures as observed through the phonon broadenings [full width half maximum (FWHM)]. Because of the fact the lattice damage only occurs at the laser written tracks and not on its surroundings, the mapping and visualization of the phonon broadening allow to directly image the depressed-cladding structure, which is extremely useful in order to demonstrate that these waveguides are indeed depressed-cladding tubular structures capable of channel confinement. Because the lower side of the images corresponds to the closer side to the sample surface, the focused laser pulses typically induce a slightly higher level of damage. This can be seen on the higher level of FWHM that the cladding structures have on this side. This effect can be easily improved by slightly decreasing the laser power for that given section of cladding structures. Although it is not observable under the inspection microscope (see Fig. 1), Figs. 2(b) and 2(c) clearly show that the cladding structure is stronger in the upper and lower parts, and this higher amount of lattice damage could be a source of anisotropy for the TM/TE modes propagation losses.

The most important result from the FWHM maps is the demonstration that the Nd:$GdVO_4$ crystal is completely undamaged in the waveguiding volume (there is no phonon broadening in the mode volume), which is a big advantage for achieving high-laser efficiency. This feature makes cladding structures the ideal design for integrated lasers, when compared with Type II or Type I waveguides, because in Type I waveguide the core region is directly modified and in Type II waveguides the modes always have to be located close to the damage tracks, therefore reducing the effective active volume of the waveguide and furthermore increasing the propagation losses because of light scattering.

Figures 2(d)–2(f) show the mapping result for the mode energy shifts of the three types of cladding designs. These phonon shifts indicate that a slight lattice distortion occurs in the surroundings of the cladding tracks. Furthermore,

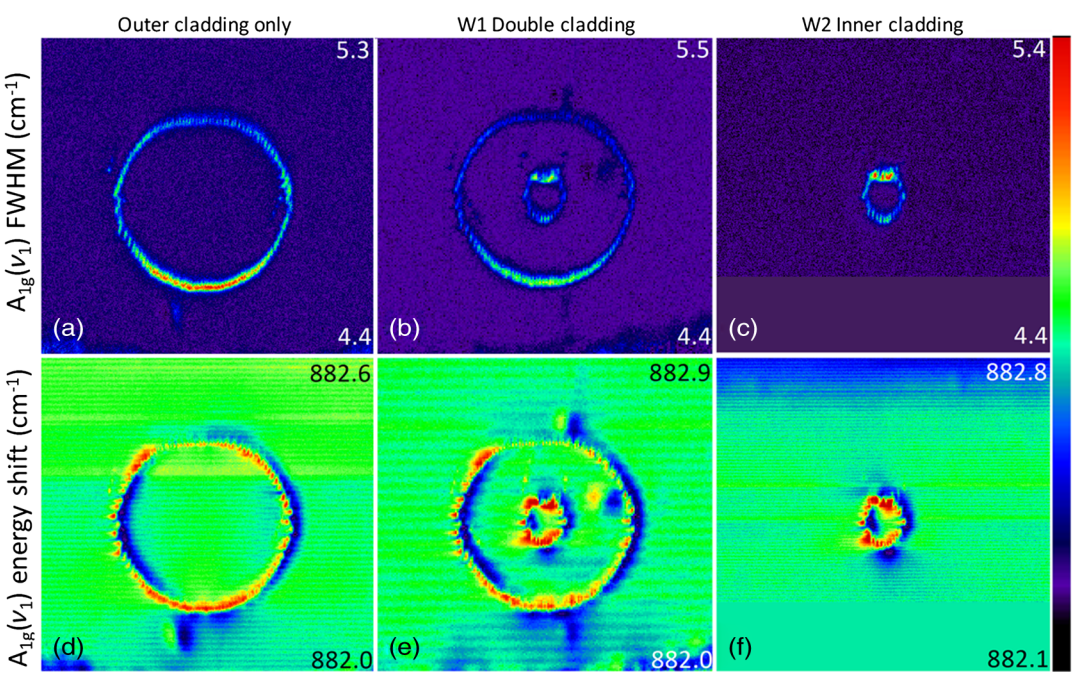


**Fig. 2** Mapping results for the three types of cladding structures. (a–c) The depressed cladding through the imaging of the phonon broadening. Inset numbers show the maximum and minimum FWHM values. (d–f) The presence of lattice distortion associated with the damage cladding. Inset numbers show the maximum and minimum energy shift values.

although the stress biaxial field associated with the fabricated claddings cannot be calculated with the available data, the phonon shift images show how the sequential fabrication of different tracks produces a strong effect of stress build-up, which is extremely important in crystalline waveguides and can entail crystal cracking. In order to better visualize the stress build-up, which occurs due to the closely lying tracks, Fig. 3 gives a closer view of a section of the cladding with the DLW damage track coordinates superimposed.

Figure 3(a) shows how the waveguide is constructed by a nearly continuous array of lower index lines, which constitute the depressed cladding structure. The width of the tracks as observed by the FWHM is of around ~2 $\mu$m. Figure 3(b) shows the corresponding energy shift of the mode. It can be observed that the phonon energy shift around the damage tracks is complex and incompletely homogeneous. The maximum and minimum values of energy shift occur for the track arrangements where the vertical distance between tracks is maximum. When the tracks start to lie close horizontally, the blue and red shifts are attenuated, most probably because of a compensation of stress fields between closely lying tracks. The effect of an asymmetric effect in the left (blue shift) and right (red shift) of the $A_{1g}(\nu_1)$ phonon-mode energy is, at this moment, still not fully understood. We disregard the effects because of laser alignment, because this would not cause such a strong asymmetry in the stress field. We state here that this nonsymmetric effect could be because of the complex crystalline structure of vanadate crystals, and the fact that the response of the $A_{1g}(\nu_1)$ phonon mode to anisotropic lattice distortions has never been reported as far as we know. Because the tetragonal $VO_4^{3-}$ ionic group is fully sensitive to 3-D lattice distortions, further studies on how the symmetric stretching-mode frequency responds to axial or biaxial distortions along the $a$, $b$, or $c$ axis need to be performed.

### 3.2 *Laser Experiments*

With the analysis of the emission spectra of the output light (see Fig. 4), we found that the typical laser oscillation from the core of the fs-laser inscribed Nd:$GdVO_4$ depressed-cladding waveguides was achieved when the absorbed power is above the lasing threshold. The central wavelength of the laser emission from the cladding waveguide is at 1064.5 nm, which corresponds to the main fluorescence of $^4F_{3/2} \rightarrow {}^4I_{11/2}$ transition in the $Nd^{3+}$ ions, with a FWHM of ~0.6 nm.

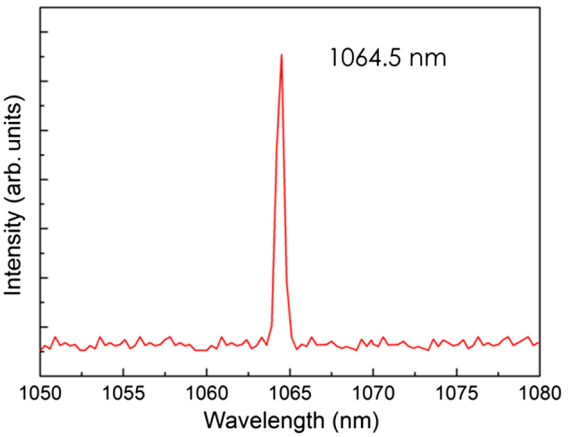


**Fig. 4** Laser emission spectrum from the fs-laser inscribed Nd:$GdVO_4$ depressed-cladding waveguides. Peak position stays at 1064.5 nm and the FWHM is 0.6 nm.

Figures 5(a)–5(d) show the distribution of the modal profiles of the laser oscillation generated from the depressed cladding waveguides under 808-nm optical pumping at room temperature. Figures 5(a) and 5(b) stand for the laser mode generated in the waveguide WG1, and Figs. 5(c) and 5(d) stand for that generated in the waveguide WG2. The horizontal and vertical arrows indicate the TE and TM polarizations, respectively. As it can be clearly seen in the figures, for both waveguide diameters and polarizations, each of the output modes exhibits highly symmetrical and circular distribution. This is different from the Type II waveguides in cubic crystals (e.g., Nd:GGG[15] or Nd:YAG[9,11,14]) and Ti:sapphire,[36] which only support guided lasers along the TM polarization. For the core waveguide in the structure of WG1 and the single-cladding waveguide WG2, the waveguide laser at 1064 nm was demonstrated to only support

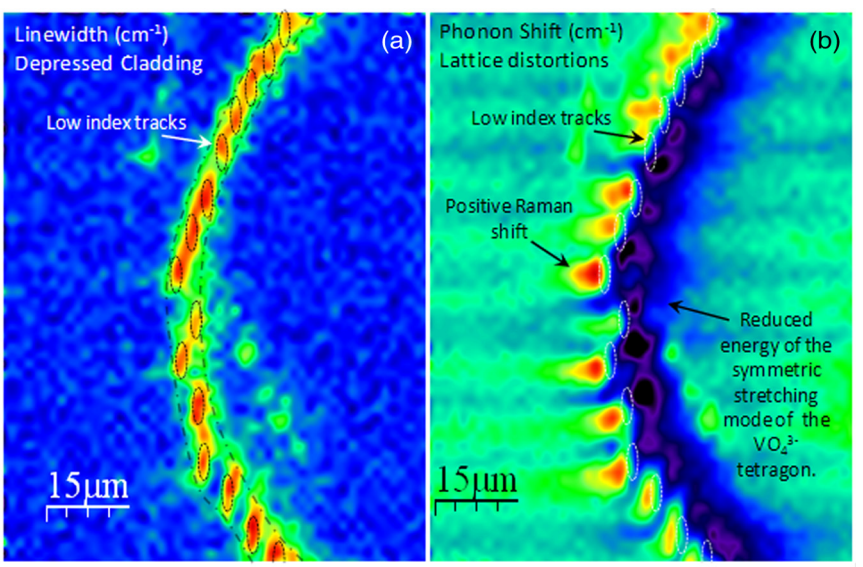


**Fig. 3** Laser-written track coordinates superimposed on the Raman maps of (a) FWHM of the Raman mode and (b) Raman energy shift of the phonon mode.

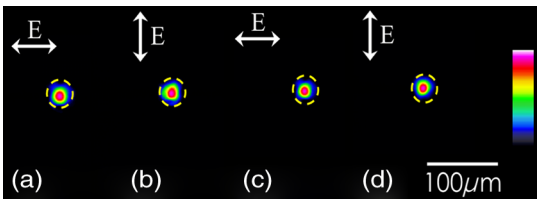


**Fig. 5** Distribution of the modal profiles of the laser oscillation collected from the depressed-cladding waveguides [(a) and (b) for WG1 and (c) and (d) for WG2] at 1064.5 nm, respectively. (a) and (c) correspond to the transverse electric (TE) polarization and (b) and (d) to the transverse magnetic (TM) polarization. The dashed lines indicate the spatial locations of the fs-laser-induced damage tracks.

zero-order mode, which makes the 30-$\mu$m diameter cladding waveguide laser a single-mode system. Compared with the dual-line Type II Nd:$GdVO_4$ waveguide lasers, the cladding waveguide mode is more symmetric.[16] The circular-depressed cladding structure makes an important contribution to the symmetric single-modal profile if compared with the anisotropic stress field in the double-line waveguide reported in our previous works.[37]

With consideration of the transmittance and reflectivity of the optical elements (e.g., microscope lenses) in the end-coupling experiment, we calculated the launched powers and the output powers.[14] Figure 6 shows the output laser powers (at wavelength of 1064.5 nm), when the spherical convex lens with a focal length of 75 mm was applied, as a function of the launched pump powers at 808 nm in the Nd:$GdVO_4$ cladding waveguides WG1 and WG2, respectively. From the linear fit of the experimental data, for the double-cladding waveguide WG1 in the Nd:$GdVO_4$ crystal, the maximum output power and lasing thresholds are $P_{WG1,TE} \approx 0.43$ W, $P_{WG1,TM} \approx 0.35$ W, $P_{TE,th} \approx 92$ mW, and $P_{TM,th} \approx 105$ mW, respectively. Meanwhile, the extracted slope efficiencies of these waveguides are $\Phi_{WG1,TE} \approx 52.3\%$ and $\Phi_{WG1,TM} \approx 49.4\%$, corresponding to optical-to-optical conversion efficiency of $\eta_{WG1,TE} \approx 47.3\%$ and $\eta_{WG1,TM} \approx 38.5\%$, respectively. As for the depressed single-cladding waveguide WG2, the slope efficiencies are $\Phi_{WG2,TE} \approx 43\%$ and $\Phi_{WG2,TM} \approx 36\%$ with maximum output power of 0.35 and 0.3 W, respectively, which correspond to an optical-to-optical conversion efficiency of $\eta_{WG2,TE} \approx 33\%$ and $\eta_{WG2,TM} \approx 26\%$. The reason for the performances of laser oscillation in the core region of double-cladding WG1 being better than those of the cw laser generated in inner cladding alone WG2 might be mainly because of the outermost cladding structure, which benefit the inner core area with the large-area pump with enhancing the slope efficiency and maximum output power. As the result of the ellipsoid-shaped configuration for the core waveguide in WG1 and WG2 companied with the stress-induced change in the waveguide area, the waveguide lasers at TE polarization show much higher efficiency than those at TM polarization for both waveguides. Nevertheless, compared with our previous results on Nd:$GdVO_4$ dual-line Type II waveguides ($P \sim 0.25$ W), the output powers of the cladding waveguides of WG1 and WG2 are of 1.7 and 1.4 times of magnitude, respectively.[17] The stable features of the present system suggest that the W-level waveguide lasing may be achieved by using higher-power diode pumping. Furthermore, by analyzing the data from Fig. 6, we could conclude that the cladding waveguides with larger diameters have much higher output laser powers than the smaller volume waveguide, which is in accordance with the previous report.[23] A rough explanation is that the smaller-diameter cladding waveguides possess lower lasing thresholds with lower coupling efficiency and synergy the effect of the round-trip cavity loss exponential factor $\delta$ and the effective pump area $A_{eff}$ of the waveguide laser system, as their impacts on the lasing threshold $P_{th}$ as the $P_{th} \propto \delta \cdot A_{eff}^2$. In addition, one may note that the diameters of the cladding waveguides are comparable with those of the multimode fibers, which are fundamental to construct highly efficient fiber-waveguide laser systems for integrated photonic applications.

## 4 Summary

We have fabricated circular-depressed double cladding waveguides with diameters of 150 and 30 $\mu$m in Nd:$GdVO_4$ crystals by multiplying inscription of fs-laser pulses. High-symmetry and high-output power (~0.43 W) laser oscillation were generated under an optical laser at 808-nm excitation. The waveguide lasers show great performance with a peak slope efficiency of 52.3% and a threshold of 92 mW. The excellent guiding and laser operation indicate the potential applications of the fs-laser inscribed Nd:$GdVO_4$ double-cladding waveguides as new efficient laser devices for integrated photonic applications.

### *Acknowledgments*

The work is supported by the National Natural Science Foundation of China (No. 11274203), the Specialized Research

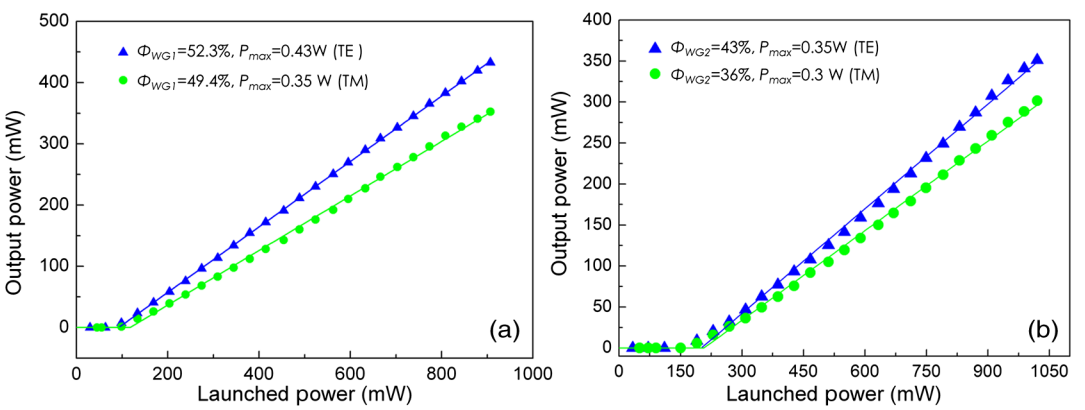


**Fig. 6** Output power at 1064.5 nm of the cw waveguide laser collected from waveguides WG1 (a) and WG2 (b) as a function of the launched power at 808 nm. The solid triangles and circles stand for the data collected at TM and TE polarizations with linear fits (solid lines).

Fund for the Doctoral Program of Higher Education of China (No. 20130131130001), and Junta de Castilla y León under project SA086A12-2. Support from the Centro de Láseres Pulsados (CLPU) is also acknowledged. This work was supported by the Spanish Government under project MAT2011-29255-C02-02 and by the Generalitat de Catalunya under project 2014SGR1358.

## References


1. E. J. Murphy, *Integrated Optical Circuits and Components*, Marcel Dekker, New York (1999).
2. C. Grivas, "Optically pumped planar waveguide lasers, Part I: fundamentals and fabrication techniques," *Prog. Quantum Electron.* **35**(6), 159–239 (2011).
3. R. R. Gattass and E. Mazur, "Femtosecond laser micromachining in transparent materials," *Nat. Photonics* **2**(4), 219–225 (2008).
4. K. M. Davis et al., "Writing waveguides in glass with a femtosecond laser," *Opt. Lett.* **21**(21), 1729–1731 (1996).
5. M. Ams et al., "Ultrafast laser written active devices," *Laser Photonics Rev.* **3**(6), 535–544 (2009).
6. F. Chen and J. R. V. de Aldana, "Optical waveguides in crystalline dielectric materials produced by femtosecond-laser micromachining," *Laser Photonics Rev.* **8**(2), 251–275 (2014).
7. A. Ródenas and A. Kar, "High-contrast step-index waveguides in borate nonlinear laser crystals by 3D laser writing," *Opt. Express* **19**(18), 17820–17833 (2011).
8. J. Burghoff, S. Nolte, and A. Tunnermann, "Origins of waveguiding in femtosecond laser structured $LiNbO_3$," *Appl. Phys. A: Mater. Sci. Process.* **89**(1), 127–132 (2007).
9. J. Siebenmorgen et al., "Femtosecond laser written stress-induced Nd:$Y_3A_{15}O_{12}$ (Nd:YAG) channel waveguide laser," *Appl. Phys. B* **97**(2), 251–255 (2009).
10. J. Siebenmorgen et al., "Highly efficient Yb:YAG channel waveguide laser written with a femtosecond-laser," *Opt. Express* **18**(15), 16035–16041 (2010).
11. A. Okhrimchuk et al., "Low loss depressed cladding waveguide inscribed in YAG:Nd single crystal by femtosecond laser pulses," *Opt. Express* **20**(4), 3832–3843 (2012).
12. G. A. Torchia et al., "Highly efficient laser action in femtosecond-written Nd:yttrium aluminum garnet ceramic waveguides," *Appl. Phys. Lett.* **92**(11), 111103 (2008).
13. T. Calmano et al., "Characterization of an Yb:YAG ceramic waveguide laser, fabricated by the direct femtosecond-laser writing technique," *Appl. Phys. B* **103**(1), 1–4 (2011).
14. N. Pavel et al., "Efficient laser emission in diode-pumped Nd:YAG buried waveguides realized by direct femtosecond-laser writing," *Laser Phys. Lett.* **10**(9), 095802 (2013).
15. C. Zhang et al., "Channel waveguide lasers in Nd:GGG crystals fabricated by femtosecond laser inscription," *Opt. Express* **19**(13), 12503–12508 (2011).
16. W. F. Silva et al., "Femtosecond-laser-written, stress-induced Nd:$YVO_4$ waveguides preserving fluorescence and Raman gain," *Opt. Lett.* **35**(7), 916–918 (2010).
17. Y. Tan et al., "70% slope efficiency from an ultrafast laser-written Nd:$GdVO_4$ channel waveguide laser," *Opt. Express* **18**(24), 24994–24999 (2010).
18. D. G. Lancaster et al., "Efficient 2.9 $\mu$m fluorozirconate glass waveguide chip laser," *Opt. Lett.* **38**(14), 2588–2591 (2013).
19. Y. Ren et al., "Mid-infrared waveguide lasers in rare-earth-doped YAG," *Opt. Lett.* **37**(16), 3339–3341 (2012).
20. G. Salamu et al., "Cladding waveguides realized in Nd:YAG ceramic by direct femtosecond-laser writing with a helical movement technique," *Opt. Mater. Express* **4**(4), 790–797 (2014).
21. G. Salamu et al., "Laser emission from diode-pumped Nd:YAG ceramic waveguide lasers realized by direct femtosecond-laser writing technique," *Opt. Express* **22**(5), 5177–5182 (2014).
22. Y. Jia et al., "Femtosecond-laser-inscribed $BiB_3O_6$ nonlinear cladding waveguide for second-harmonic generation," *Appl. Phys. Express* **5**(7), 072701 (2012).
23. Y. Jia, F. Chen, and J. R. V. de Aldana, "Efficient continuous-wave laser operation at 1064 nm in Nd:$YVO_4$ cladding waveguides produced by femtosecond laser inscription," *Opt. Express* **20**(15), 16801–16806 (2012).
24. Y. Ren et al., "Channel waveguide lasers in Nd:LGS crystals," *Opt. Express* **21**(5), 6503–6508 (2013).
25. G. Palmer et al., "High slope efficiency and high refractive index change in direct-written Yb-doped waveguide lasers with depressed claddings," *Opt. Express* **21**(14), 17413–17420 (2013).
26. A. Arriola et al., "Low bend loss waveguides enable compact efficient 3D photonic chips," *Opt. Express* **21**(3), 2978–2986 (2013).
27. A. A. Kaminskii, "Laser crystals and ceramics: recent advances," *Laser Photonics Rev.* **1**(2), 93–177 (2007).
28. L. Fornasiero et al., "Excited state absorption and stimulated emission of $Nd^{3+}$ in crystals. Part 2: $YVO_4$, $GdVO_4$, and $Sr_5(PO_4)_3F$," *Appl. Phys. B* **67**(5), 549–553 (1998).
29. V. Ostroumov et al., "Study of luminescence concentration quenching and energy transfer upconversion in Nd-doped $LaSc_3(BO_3)_4$ and $GdVO_4$ laser crystals," *J. Opt. Soc. Am. B* **15**(3), 1052–1060 (1998).
30. H. J. Zhang et al., "Investigations on the growth and laser properties of Nd:$GdVO_4$ single crystal," *Cryst. Res. Technol.* **33**(5), 801–806 (1998).
31. N. Dong, Y. Yao, and F. Chen, "Optical waveguides in Nd:$GdVO_4$ crystals fabricated by swift $N^{3+}$ ion irradiation," *Opt. Mater.* **35**(2), 310–313 (2012).
32. H. Li et al., "Nd:$GdVO_4$ thin films grown on LaGaSiO (LGS) and sapphire substrates by pulsed laser deposition properties," *J. Cryst. Growth* **281**(2–4), 426–431 (2005).
33. R. Ramponi, R. Osellame, and M. Marangoni, "Two straightforward methods for the measurement of optical losses in planar waveguides," *Rev. Sci. Instrum.* **73**(3), 1117–1120 (2002).
34. A. A. Kaminskii et al., "Crystal-host $Gd_{0.5}Lu_{0.5}VO_4$ for $Ln^{3+}$-lasants: a new high-gain many-phonon $\chi(3)$-active tetragonal vanadate-SRS spectroscopy and nonlinear-laser effects," *Appl. Phys. B* **109**(4), 649–658 (2012).
35. A. Ródenas et al., "Refractive index change mechanisms in femtosecond laser written ceramic Nd:YAG waveguides: micro-spectroscopy experiments and beam propagation calculations," *Appl. Phys. B* **95**(1), 85–96 (2009).
36. C. Grivas et al., "Tunable, continuous-wave Ti:sapphire channel waveguide lasers written by femtosecond and picosecond laser pulses," *Opt. Lett.* **37**(22), 4630–4632 (2012).
37. G. A. Torchia et al., "Highly efficient laser action in femtosecond-written Nd:yttrium aluminum garnet ceramic waveguides," *Appl. Phys. Lett.* **92**(11), 111103 (2008).


**Hongliang Liu** received his BA degree from Shandong University, Jinan, China, in 2011. He is currently working toward the PhD degree at the same university. His current research interests include fabrication of optical waveguides in laser materials by using ion beam implantation and femtosecond laser inscription technique.

**Javier R. Vázquez de Aldana** received his bachelor of science (1997) and PhD (2001) from University of Salamanca, Spain. He is currently an associate professor of the same university. His research activity is focused on the interaction of intense femtosecond pulses with materials and its application on fabrication of photonic devices. He is a member of Laser Microprocessing Research Group and also a technical and scientific advisor of Laser Facility at University of Salamanca.

**Magdalena Aguiló** received the BSc and PhD degrees from University of Barcelona, Barcelona, Spain. Currently, she is a full professor of crystallography at University Rovira i Virgili (URV), Tarragona, Spain. Her research interests include structural characterization of crystalline materials, x-ray diffraction and synchotron, anisotropy of the physical properties in relation with crystalline structure, etc. She is a coauthor of 256 papers and two registered and transferred patents. She received the Professor Distingit award by URV (2013).

**Francesc Díaz** earned his BSc degree in physics in 1976 and a PhD degree in physics in 1982 at the University of Barcelona. He is a full professor of applied physics at Universitat Rovira i Virgili since 1992 and leader of the research group of Physics and Crystallography of Materials (FiCMA). His research interests are currently focused in two subjects: nanoparticles and nanostructured materials for integrated optics, and photonic devices from laser, nonlinear optics, and photonic crystals.

**Feng Chen** is a professor at Shandong University, China. He received the PhD degree from Shandong University in 2002. He was with Clausthal University of Technology, Germany, from 2003 to 2005, as a Humboldt research fellow. He has published about 200 papers in peer-reviewed journals. He is a fellow of the Institute of Physics, UK, a senior member of the OSA, and a member of SPIE. He also serves as an associate editor of *Optical Engineering*.

**Airán Ródenas Seguí** graduated with a PhD degree from Universidad Autónoma de Madrid, Spain, in 2009. In 2010, he joined at Heriot-Watt University as a postdoctoral research associate. In 2012, he joined Universitat Rovira i Virgili, Spain, as a research associate. His research activity covers micro-spectroscopy techniques and ultrashort pulse laser processing of materials. He is a main author of a patent on a laser-written MIR photonic sensor for early alert of surface ice nucleation.